

# Journal of Materials Chemistry C

Accepted Manuscript



This is an *Accepted Manuscript*, which has been through the Royal Society of Chemistry peer review process and has been accepted for publication.

*Accepted Manuscripts* are published online shortly after acceptance, before technical editing, formatting and proof reading. Using this free service, authors can make their results available to the community, in citable form, before we publish the edited article. We will replace this *Accepted Manuscript* with the edited and formatted *Advance Article* as soon as it is available.

You can find more information about *Accepted Manuscripts* in the [Information for Authors](#).

Please note that technical editing may introduce minor changes to the text and/or graphics, which may alter content. The journal's standard [Terms & Conditions](#) and the [Ethical guidelines](#) still apply. In no event shall the Royal Society of Chemistry be held responsible for any errors or omissions in this *Accepted Manuscript* or any consequences arising from the use of any information it contains.

# Sandwich-structured Fe<sub>2</sub>O<sub>3</sub>@SiO<sub>2</sub>@Au nanoparticles with magnetoplasmonic responses

Zhongyu Cai,<sup>a,b\*</sup> Eunice S. P. Leong,<sup>c</sup> Zhigang Wang,<sup>a</sup> Wenxin Niu,<sup>a</sup> Weiqing Zhang,<sup>a</sup> Serge Ravaine,<sup>d</sup> Nikolai L. Yakovlev,<sup>c</sup> Yan Jun Liu,<sup>c\*</sup> Jinghua Teng,<sup>c\*</sup> Xianmao Lu<sup>a\*</sup>

<sup>5</sup> Received (in XXX, XXX) Xth XXXXXXXXXX 20XX, Accepted Xth XXXXXXXXXX 20XX

DOI: 10.1039/b000000x

We report a method for the fabrication of relatively uniform sandwich-like core-interlayer-shell nanostructures by using  $\gamma$ -Fe<sub>2</sub>O<sub>3</sub> as the inner core, SiO<sub>2</sub> as the interlayer, and relatively uniform Au as the outer shell. The resulting novel hybrid nanoparticle combines the intense local fields of nanorods with the highly tunable plasmon resonances of nanoshells. The length and diameter of the resulting nanoparticles can be tuned by the aspect ratio of  $\alpha$ -Fe<sub>2</sub>O<sub>3</sub>, the interlayer of SiO<sub>2</sub> and outer layer of Au. After calcination under H<sub>2</sub> and then exposure to air, the  $\alpha$ -Fe<sub>2</sub>O<sub>3</sub> was transformed into  $\gamma$ -Fe<sub>2</sub>O<sub>3</sub>, which endows the hybrid particle magnetic tunability. This metal oxides ( $\gamma$ -Fe<sub>2</sub>O<sub>3</sub>) dielectric core, SiO<sub>2</sub> interlayer and gold (Au) shell spindle nanoparticle resembles to a grain of Au nanorice ( $\gamma$ -Fe<sub>2</sub>O<sub>3</sub>@SiO<sub>2</sub>@Au ellipsoids). The core-interlayer-shell geometry possesses greater structural and magnetic tunability than either a nanorod or a nanoshell. The plasmon resonance of this novel  $\gamma$ -Fe<sub>2</sub>O<sub>3</sub>@SiO<sub>2</sub>@Au geometry is believed to arise from a hybridization of the primitive plasmons of an ellipsoidal cavity inside a continuous Au shell. The unique magnetoplasmonic properties of this  $\gamma$ -Fe<sub>2</sub>O<sub>3</sub>@SiO<sub>2</sub>@Au nanostructure are highly attractive for applications such as surface plasmon resonance sensing because of the dipole resonance of the resultant nanostructure and recyclable catalysts arising from the outer Au layer and inner magnetic  $\gamma$ -Fe<sub>2</sub>O<sub>3</sub> core.

## 1. Introduction

Core-shell nanostructures that combine the properties of both the core and shell materials have attracted intense research interest in recent years due to their potential in various applications in renewable energy, environmental cleanup, biomedicine, nanophotonics and energy storage.<sup>1-12</sup> In general, core-shell nanoparticles (NPs) can be classified into dielectric core@dielectric shell, metal core@dielectric shell, and metal core@metal shell structures.<sup>13</sup> The rapid development in plasmonics has intrigued novel dielectric core@metal shells because of the more flexibility in engineering their plasmonic properties. Plasmonic dielectric core@metal shell NPs have strong optical absorption and scattering properties, which can span a large region of the electromagnetic spectrum from visible to the far-infrared.<sup>14, 15</sup> The remarkable plasmonic properties of these types of NPs have led to numerous applications, from fluorescence enhancement of weak molecular emitters, substrates for surface plasmon resonance (SPR) sensing, biosensing, surface enhanced Raman and surface enhanced infrared absorption spectroscopies, to contrast enhancement in bioimaging and photothermal cancer therapy.<sup>2-6, 8, 16</sup>

The root of the remarkable plasmonic properties of this kind of NPs is their geometry-dependent, plasmon-derived optical resonances whose frequencies depend sensitively on the inner and outer dimensions of their metallic shell layers. Various methods have been developed for the fabrication of dielectric core@metal shell NPs.<sup>5</sup> Halas and co-workers pioneered the fabrication of dielectric core@metal shell NPs.<sup>6, 14, 17</sup> In their method, the surface of dielectric core was first functionalized with an organosilane derivative bearing amine functional group. Then the core is attached with tiny gold (Au) NPs. Finally, a plating

solution is used to grow Au layers on the core.<sup>17</sup> By using this method, a relatively complete Au shells can be fabricated. This method is feasible in the fabrication of dielectric core@Au shell NPs. Recently, some other investigators also tried to fabricate such a dielectric core@metal shell structure with different methods. Yu and co-authors reported the synthesis, characterization and properties of  $\alpha$ -Fe<sub>2</sub>O<sub>3</sub>@SiO<sub>2</sub>/Au NPs, in which hematite cubic  $\alpha$ -Fe<sub>2</sub>O<sub>3</sub> was firstly coated with one layer of SiO<sub>2</sub>.<sup>18</sup> The resulting spherical structure was then attached with Au NPs.<sup>18</sup> In another study, Peng *et al.* described the synthesis of spherical  $\gamma$ -Fe<sub>2</sub>O<sub>3</sub>/SiO<sub>2</sub>/Au magnetic composites with sparse Au nanoparticle on the surface of SiO<sub>2</sub> layer.<sup>19</sup> Liz-Marzán *et al.* and Ma *et al.* have demonstrated the fabrication of spindle-like  $\alpha$ -Fe<sub>2</sub>O<sub>3</sub>@Au NPs, respectively, using a similar layer-by-layer assembly method combining with seed growth method.<sup>20, 21</sup> A continuous Au shell has been fabricated through an adsorption and a subsequent metallization on Au-seeded APTES-grafted silica spheres. But the resulting Au shell is still very rough which leads to a broad plasmonic peak.<sup>22</sup> In spite of these studies, the fabrication of NPs with instantaneous and reversible tuning of the plasmonic property remains a challenge. Furthermore, future development in this area requires these plasmonic NPs to possess versatile structure and tunable electrical, optical or magnetic properties.<sup>23-25</sup>

Here we report a spindle-like hybrid nanostructure geometry that combines the plasmonic properties of both magnetic nanorods and noble metallic nanoshells in a single structure. Uniform sandwich-like core-interlayer-shell NPs are fabricated by using  $\gamma$ -Fe<sub>2</sub>O<sub>3</sub> ellipsoids as the inner core, SiO<sub>2</sub> as the interlayer, and uniform Au as the outer shells (Scheme 1), which is different from previously reported  $\alpha$ -Fe<sub>2</sub>O<sub>3</sub>@Au nanostructure due to its magnetic core.<sup>17, 20, 21</sup> In this hybrid nanostructure,  $\alpha$ -Fe<sub>2</sub>O<sub>3</sub> ellipsoids with different aspect ratios were firstly

synthesized by the precipitation of iron (III) perchlorate in the presence of urea. The ellipsoids were then modified with PVP and coated with SiO<sub>2</sub> via a modified Stöber method.<sup>26-28</sup> The core-shell NPs were reduced by H<sub>2</sub> and the ellipsoids became magnetic. Finally, the Au shell was grown on the surface of the  $\gamma$ -Fe<sub>2</sub>O<sub>3</sub>@SiO<sub>2</sub> NPs with different thicknesses by varying the amount of Au plating solution added. Such hybrid nanostructures possess both magnetic and plasmonic properties, indicating that they could be actively controlled by a magnetic field and hence are important for active plasmonics and recyclable catalysts.

## 2. Experimental section

**2.1 Materials.** Iron(III) perchlorate (Fe(ClO<sub>4</sub>)<sub>3</sub>·6H<sub>2</sub>O, Reagent Grade), sodium dihydrogen phosphate (NaH<sub>2</sub>PO<sub>4</sub>, Technical Grade), urea (NH<sub>2</sub>CONH<sub>2</sub>), poly (vinyl pyrrolidone) with average molar mass of 360 kg/mol (PVP, K90), tetraethoxysilane (TEOS, 98%), tetramethylammonium hydroxide aqueous solution (TMAH, v/v, 10%), ethanol (≥99.7%), (3-aminopropyl) trimethoxysilane (APTMS, 97%), tetrachloroauric acid (HAuCl<sub>4</sub>·3H<sub>2</sub>O), absolute ethanol, tetrakis hydroxymethyl phosphonium chloride (THPC) were purchased from Sigma-Aldrich. Chloroauric acid and potassium dihydrogen phosphate (KH<sub>2</sub>PO<sub>4</sub>) were obtained from Fisher Scientific (Hampton, NH). All the chemicals were used as received without further purification. Ultrapure water (18.2 MΩ resistivity) was obtained from a Milli-Q water purification system (Millipore, Billerica, MA). (*Caution! Ethanol, CO, chloroauric acid, THPC, APTMS, APTES, and piranha present potential health and/or fire hazards. Appropriate precautions should be observed at all times.*)

### 2.2 Preparation of $\gamma$ -Fe<sub>2</sub>O<sub>3</sub>@SiO<sub>2</sub>@Au NPs

Generally, there are four steps (Scheme 1) in the fabrication of  $\gamma$ -Fe<sub>2</sub>O<sub>3</sub>@SiO<sub>2</sub>@Au NPs with tailored plasmon resonance: (1) synthesis of spindle-like  $\alpha$ -Fe<sub>2</sub>O<sub>3</sub>; (2) coating of SiO<sub>2</sub> onto the surface of  $\alpha$ -Fe<sub>2</sub>O<sub>3</sub>; (3) transformation of  $\alpha$ -Fe<sub>2</sub>O<sub>3</sub>@SiO<sub>2</sub> into  $\gamma$ -Fe<sub>2</sub>O<sub>3</sub>@SiO<sub>2</sub> and attachment of colloidal Au NPs; 4) plating of Au onto the seeded  $\gamma$ -Fe<sub>2</sub>O<sub>3</sub>@SiO<sub>2</sub> NPs.

#### 2.2.1 Preparation of $\alpha$ -Fe<sub>2</sub>O<sub>3</sub> NPs

Uniform  $\alpha$ -Fe<sub>2</sub>O<sub>3</sub> ellipsoids with different aspect ratios were synthesized by precipitation of iron (III) perchlorate in the presence of urea.<sup>29</sup> Briefly, 4.62 g Fe(ClO<sub>4</sub>)<sub>3</sub> · 6H<sub>2</sub>O together with 0.036 g NaH<sub>2</sub>PO<sub>4</sub> and 0.60 g urea were dissolved in 100 mL deionized water in a triangular flask under ultrasonication at room temperature. The solution was kept undisturbed in an oven for 24 h at 100 °C before it was cooled slowly to room temperature. Centrifugation was applied to the dispersion to purify the hematite spindles at 6000 rpm, 30 min for six times,

until a transparent supernatant was observed. By varying the ratio between Fe(ClO<sub>4</sub>)<sub>3</sub> · 6H<sub>2</sub>O and NaH<sub>2</sub>PO<sub>4</sub>, the aspect ratio of Fe<sub>2</sub>O<sub>3</sub> ellipsoids can be precisely controlled.

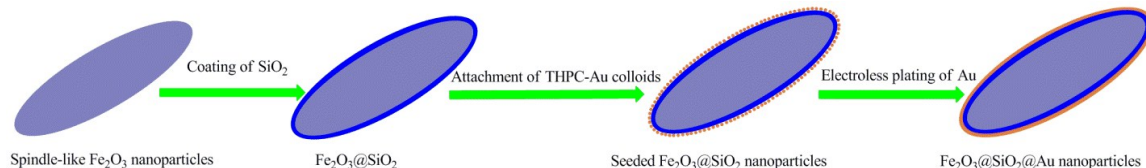
#### 2.2.2 Preparation of $\alpha$ -Fe<sub>2</sub>O<sub>3</sub>@SiO<sub>2</sub> and $\gamma$ -Fe<sub>2</sub>O<sub>3</sub>@SiO<sub>2</sub> NPs

We modified the surface of hematite cores with PVP, followed by silica coating with Stöber method via the hydrolysis of TEOS (98%).<sup>30</sup> Specifically, 1.2 g PVP K90 were added to the dispersion (containing 0.1 g  $\alpha$ -Fe<sub>2</sub>O<sub>3</sub>) to keep the hematite spindle stable, followed by centrifugation (8000 rpm for 40 min) to remove the unabsorbed PVP molecules. Silica coating of the spindle hematite (0.1 g) was carried out in 100 mL ethanol in the presence of 6 mL water and 0.2 mL TMAH (v/v 10%) as the base catalyst. 2 mL of TEOS were added to the system every 2 h for certain times to achieve different aspect ratios. Strong ultrasonication was applied during the coating process to prevent the spindles from crosslinking. The ellipsoids with maghemite core were obtained by reducing the hematite core under H<sub>2</sub> at 360 °C for 4 h, followed by exposure to the air at 240 °C for 2 h. After calcination, the ellipsoids were redispersed in ethanol under ultrasonication for 4 h.

#### 2.2.3 Preparation of $\gamma$ -Fe<sub>2</sub>O<sub>3</sub>@SiO<sub>2</sub>@Au NPs

The seed particles ( $\gamma$ -Fe<sub>2</sub>O<sub>3</sub>@SiO<sub>2</sub>@THPC-Au) used in the present study were fabricated following a similar procedure as the method for the immobilization of Au NPs on silica surfaces.<sup>17</sup> The surface of the spindle-shaped  $\gamma$ -Fe<sub>2</sub>O<sub>3</sub>@SiO<sub>2</sub> particles was functionalized with organosilane molecules (APTMS) to generate an amine moiety-coated surface. Typically, 600  $\mu$ L of APTMS was introduced into 5 mL of ethanol solution of  $\gamma$ -Fe<sub>2</sub>O<sub>3</sub>@SiO<sub>2</sub> particles under vigorous stirring. The surface functionalization of  $\gamma$ -Fe<sub>2</sub>O<sub>3</sub>@SiO<sub>2</sub> particles was accomplished by stirring the mixture for 12 h. The resulting particles were centrifuged and redispersed in ethanol several times to remove the excess APTMS. THPC-capped Au NPs (~2 nm in diameter) were prepared following Duff's method,<sup>31</sup> and then attached to the functionalized  $\gamma$ -Fe<sub>2</sub>O<sub>3</sub>@SiO<sub>2</sub> particle surfaces through Au-amine interaction.<sup>32</sup> These attached Au colloids acted as the nucleation sites for the reduction of Au ions from solution onto the  $\gamma$ -Fe<sub>2</sub>O<sub>3</sub>@SiO<sub>2</sub> surface until continuous and complete Au nanoshells were formed.<sup>14</sup>

The  $\gamma$ -Fe<sub>2</sub>O<sub>3</sub>@SiO<sub>2</sub>@Au NPs were fabricated via seed-catalyzed reduction of AuCl<sub>4</sub><sup>-</sup> ions by CO in aqueous solutions at room temperature. A 44  $\mu$ M aqueous HAuCl<sub>4</sub> plating solution



**Scheme 1** Schematic illustration of hematite-SiO<sub>2</sub>-Au core-interlayer-shell NPs.

was prepared by the addition of 3 mL of 1 wt%  $\text{HAuCl}_4$  to 200 mL of 1.8 mM aqueous  $\text{K}_2\text{CO}_3$  and was stored for a minimum of 24 h before use. For a typical process, certain amount of  $\gamma\text{-Fe}_2\text{O}_3@/\text{SiO}_2@/\text{THPC-Au}$  was added into a small glass vial containing 3 mL  $\text{HAuCl}_4$  plating solution. The growth of complete Au shells typically took 5 min. By adjusting the amount ratio between seed particles and  $\text{AuCl}_4^-$  ions, the thickness of the Au shells can be precisely controlled. The resulting  $\gamma\text{-Fe}_2\text{O}_3@/\text{SiO}_2@/\text{Au}$  NPs can be homogeneously dispersed in water to form colloidal solutions.

**2.3 Characterization.** Scanning electron microscope (SEM) images were obtained on a JEOL JSM-6700F field emission SEM (FESEM) at an acceleration voltage of 5.0 kV. The samples for SEM measurements were prepared by drying a drop of colloidal solutions on silicon wafer surface. Transmission electron microscopy (TEM) and selected area electron diffraction (SAED) images were obtained using JEOL JEM-2100F transmission electron microscope at an acceleration voltage of 200 kV. X-ray diffraction (XRD) patterns were recorded on a Shimadzu XRD-6000 X-ray diffractometer using a Cu K $\alpha$  as irradiation source, operated at 40 kV and 30 mA. The magnetic properties of the samples were measured using superconducting quantum interference device (SQUID) magnetometer under an in-plane applied magnetic field between -10,000 to 10,000 Oe at room temperature. The  $\gamma\text{-Fe}_2\text{O}_3@/\text{SiO}_2@/\text{Au}$  NPs with different geometries were dispersed into water to measure their transmission in solution. Then 3 mL  $\gamma\text{-Fe}_2\text{O}_3@/\text{SiO}_2@/\text{Au}$  NPs solution was put into a fused quartz cuvette with a path length of 1 cm. The transmission spectra were obtained using a Cary 5000 UV/Vis/NIR spectrophotometer in the wavelength range of 400 nm to 2400 nm. To investigate the angular effect of a magnetic field, the measurement of the optical transmissions was performed by applying an external magnetic field with surface magnetic strength of 3600 Gauss to the solutions. The probe was perpendicular to the glass vessel and parallel to the direction of the magnetic field. Compositional investigation for the samples was carried out using X-ray photoelectron spectroscopy (XPS, AXIS-HSi, Kratos Analytical). The X-ray photoelectron spectra of the studied elements were calibrated with the C1s peak arising from adventitious carbon with a binding energy of 284.6 eV.

**2.4 Simulation.** To understand the optical response of the  $\text{Fe}_2\text{O}_3@/\text{SiO}_2@/\text{Au}$  nanoparticle, we modelled a single  $\text{Fe}_2\text{O}_3@/\text{SiO}_2@/\text{Au}$  spindle as an ellipse with longitudinal diameter of 340 nm and transverse diameter of 54 nm. The thickness of the  $\text{SiO}_2$  layer was set as 12 nm whereas the outer Au shell layer thickness is 16 nm. The n-k value of  $\text{Fe}_2\text{O}_3$  is obtained from the reference.<sup>33</sup> A fine mesh of 5 nm is applied to the structure. PML boundary conditions are applied in x-y-z directions and both the scattering and absorption of light from the spindle is calculated to determine the extinction of light. As the measurement is carried out with unpolarized light, both the x and y polarization are calculated to determine the scattering using unpolarized light. It is found that the scattering is mainly influenced by the x polarized light (i.e., polarization along the longitudinal direction). The electric field and magnetic field

distribution at the two peaks are also plotted for the x polarization.

### 3. Results and Discussion

#### 3.1 $\alpha\text{-Fe}_2\text{O}_3$ NPs with different aspect ratios

Hematite spindles with different aspect ratios were synthesized by forced hydrolysis of iron salt. The sizes and shapes of the products were characterized with TEM. The aspect ratio ( $c/a$ ) of spindle is defined as the ratio of major axis length ( $c$ ) to minor axis width ( $a$ ). The recipe is shown in Table 1. It has been reported that the molar ratio between  $\text{Fe}^{3+}$  and  $\text{H}_2\text{PO}_4^-$  has a great influence on the aspect ratio of spindles.<sup>29</sup>

**Table 1** The experimental recipes for the preparation of hematite spindles at 100 °C for 24 h

Sample	Aspect ratio	$\text{Fe}^{3+}/\text{H}_2\text{PO}_4^-$	$\text{Fe}(\text{ClO}_4)_3 \cdot 6\text{H}_2\text{O}$ (g·L <sup>-1</sup> )	$\text{NaH}_2\text{PO}_4$ (g·L <sup>-1</sup> )	Urea(g·L <sup>-1</sup> )
1	9:1	13.3	46.2	0.900	6.0
2	6:1	18.4	46.2	0.650	6.0
3	4:1	23.1	46.2	0.520	6.0
4	3:1	33.3	46.2	0.360	6.0

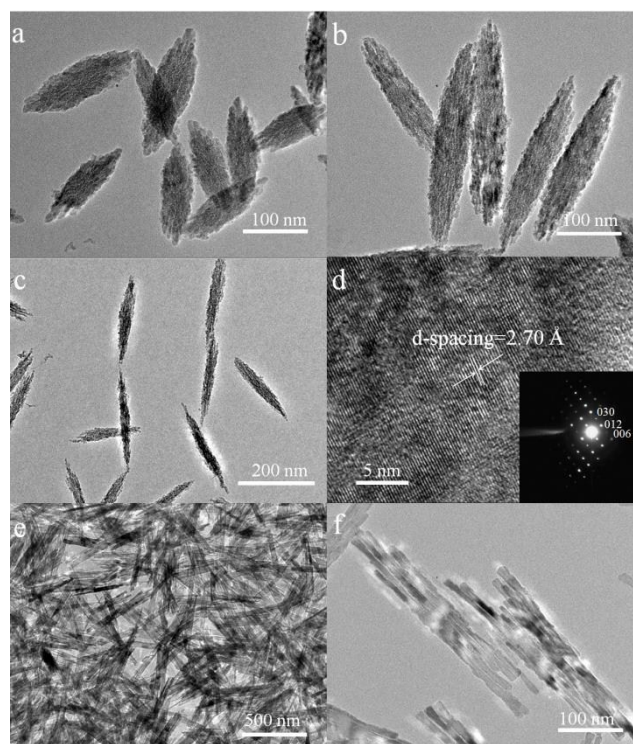


**Fig. 1** TEM images of  $\alpha\text{-Fe}_2\text{O}_3$  NPs with aspect ratios of (a) 3, (b) 6, and (c) 9; (d) HRTEM of the  $\alpha\text{-Fe}_2\text{O}_3$  NPs (the inset shows the SAED pattern of the hematite spindles); (e-f)  $\alpha\text{-Fe}_2\text{O}_3$  NPs with aspect ratio larger than 12.

By decreasing the  $\text{Fe}^{3+}/\text{H}_2\text{PO}_4^-$  molar ratio from 33.3 to 13.3, the aspect ratio of spindles can be increased as indicated in Figures 1a–c. Moreover, as shown in Figures 1a–c and summarized in Table S1, large quantity of uniform spindles with narrow size distribution (<10%) were obtained, which also can be

confirmed from the SEM image (Figure S1, ESI). Further investigation of the crystalline information of the hematite spindles was carried out with high resolution TEM (HRTEM), as shown in Figure 1d, which verified the hematite spindles to be single crystal with rhombohedral phase as reported in literature.<sup>29</sup> The d-spacing of the lattice 0.27 nm, corresponds to (104) face of  $\alpha$ -Fe<sub>2</sub>O<sub>3</sub>. The inset SAED pattern of Figure 1d further confirms the single crystalline of  $\alpha$ -Fe<sub>2</sub>O<sub>3</sub> with rhombohedral phase. It should be mentioned that further decrease of the Fe<sup>3+</sup>/H<sub>2</sub>PO<sub>4</sub><sup>3-</sup> molar ratio to 12 leads to the formation of bamboo-like hematite with a relatively large aspect ratio (Figures 1e and f). To our best knowledge, this is the first finding in the synthesis of  $\alpha$ -Fe<sub>2</sub>O<sub>3</sub>. The investigation of the mechanism is in progress.

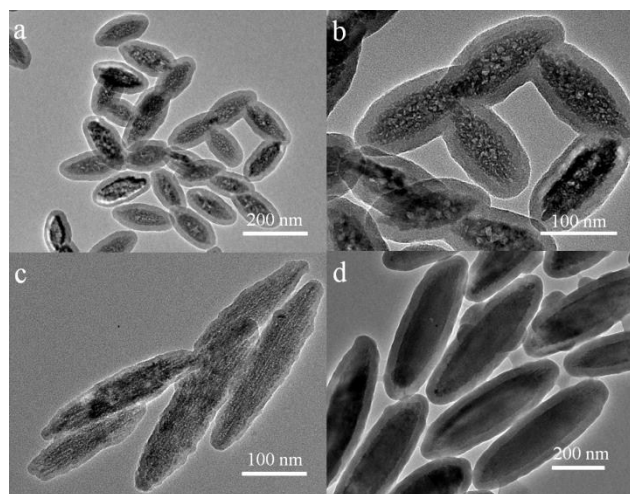


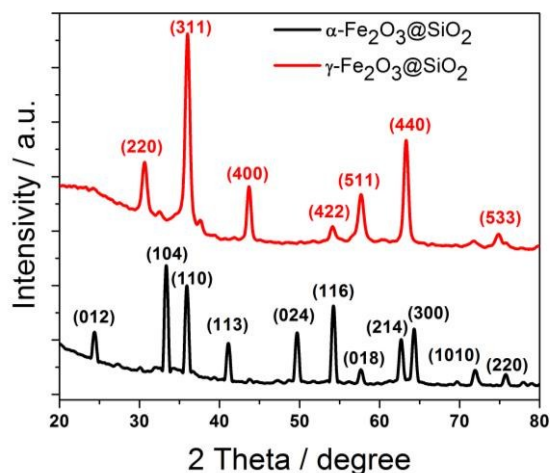
**Fig. 2** TEM images of the fabricated  $\alpha$ -Fe<sub>2</sub>O<sub>3</sub>@SiO<sub>2</sub>. (a)  $\alpha$ -Fe<sub>2</sub>O<sub>3</sub>@SiO<sub>2</sub> at low magnification (aspect ratio of 3); (b)  $\alpha$ -Fe<sub>2</sub>O<sub>3</sub>@SiO<sub>2</sub> (aspect ratio of 3) with an average shell thickness of 22.6 nm; (c)  $\alpha$ -Fe<sub>2</sub>O<sub>3</sub>@SiO<sub>2</sub> (aspect ratio of 6) with an average shell thickness of 11.8 nm; (d)  $\alpha$ -Fe<sub>2</sub>O<sub>3</sub>@SiO<sub>2</sub> (aspect ratio of 6) with an average shell thickness of 33.5 nm.

### 3.2 $\alpha$ -Fe<sub>2</sub>O<sub>3</sub>@SiO<sub>2</sub> and $\gamma$ -Fe<sub>2</sub>O<sub>3</sub>@SiO<sub>2</sub> NPs

The most frequently used coupling agent for coating colloidal particles with one layer of SiO<sub>2</sub> is PVP.<sup>34</sup> It is believed that PVP molecules behave not only as an absorbent of TEOS, but also as a surface stabilizer of spindles. It is well known that SiO<sub>2</sub> coating offers possibilities for the shape control of a particle. The smooth SiO<sub>2</sub> surface enables the advantage of coating a smooth Au shell. The silica coating procedure is in fact a process of hydrolysis of TEOS on the surface of spindle cores in the manner of layer-by-layer.<sup>27, 35</sup> To avoid the self-nucleation of the silica spheres, the amount of TEOS needs to be precisely controlled in each addition.<sup>26</sup>

Figure 2 shows the TEM images of  $\alpha$ -Fe<sub>2</sub>O<sub>3</sub>@SiO<sub>2</sub> ellipsoids with different aspect ratios and SiO<sub>2</sub> shell thickness. As shown in Figure 2a, by coating with SiO<sub>2</sub>, the rough surface of  $\alpha$ -Fe<sub>2</sub>O<sub>3</sub> becomes smooth SiO<sub>2</sub> surface of  $\alpha$ -Fe<sub>2</sub>O<sub>3</sub>@SiO<sub>2</sub> ellipsoids. The thickness of the SiO<sub>2</sub> layer can be easily tuned by varying the amount of TEOS added into the  $\alpha$ -Fe<sub>2</sub>O<sub>3</sub> solution. Thick SiO<sub>2</sub> coating can be achieved by repeating addition of TEOS. It is found that the shell thickness is ~23 nm when adding 50  $\mu$ L TEOS into a solution containing 0.05 g  $\alpha$ -Fe<sub>2</sub>O<sub>3</sub>. As shown in Figure 2b, the aspect ratio of the resulting  $\alpha$ -Fe<sub>2</sub>O<sub>3</sub>@SiO<sub>2</sub> drops from ~3 for bare hematite spindle cores to ~2 with increasing the amount of TEOS. Figures 2c and d clearly demonstrate the core-shell architecture of the synthesized ellipsoids with an aspect ratio of 6. As shown in the TEM images, the thickness of silica shell varied from 11 to 33 nm for different samples after several cycles of SiO<sub>2</sub> coating. Comparing the lengths and widths of spindles after each cycle of SiO<sub>2</sub> coating, it is found that the size increase leads to a uniform coating of SiO<sub>2</sub> on  $\alpha$ -Fe<sub>2</sub>O<sub>3</sub> NPs. In addition, the polydispersities in both length and width decrease with the increasing amount of added TEOS. After adding certain amount of TEOS, the polydispersity decreases below 5% as shown in Figure 2, which is considered as the size polydispersity of individual unit cell building blocks in three-dimensional photonic crystals. Thus, the relatively monodisperse NPs may also find applications in photonic crystals.<sup>24, 27, 36</sup>

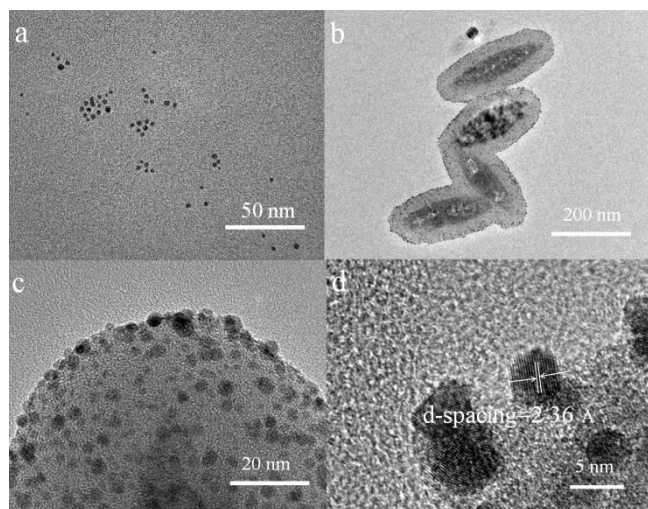
The XRD patterns of  $\alpha$ -Fe<sub>2</sub>O<sub>3</sub>@SiO<sub>2</sub> and  $\gamma$ -Fe<sub>2</sub>O<sub>3</sub>@SiO<sub>2</sub> NPs are shown in Figure 3. Characteristic diffraction peaks corresponding to  $\alpha$ -Fe<sub>2</sub>O<sub>3</sub> (012), (104), (110), (113), (024), (116), (018), (214), (300), (1010), (220) reflections can be found at  $2\theta = 24.149, 33.161, 35.629, 40.862, 49.463, 54.073, 57.607, 62.436, 63.998, 71.960, 75.451$ , respectively. In addition, the XRD pattern of the hematite spindle is also indexed to a rhombohedral phase (JCPDS No. 86-0550) and no other impurities such as FeOOH,  $\gamma$ -Fe<sub>2</sub>O<sub>3</sub> and Fe<sub>3</sub>O<sub>4</sub> can be seen here. After calcination under H<sub>2</sub> and then exposure to air, the  $\alpha$ -Fe<sub>2</sub>O<sub>3</sub>@SiO<sub>2</sub> ellipsoids were transformed into  $\gamma$ -Fe<sub>2</sub>O<sub>3</sub>@SiO<sub>2</sub> ellipsoids as confirmed by the XRD pattern. The XRD pattern of  $\gamma$ -Fe<sub>2</sub>O<sub>3</sub>@SiO<sub>2</sub> NPs is also demonstrated in Figure 3, matching  $\gamma$ -Fe<sub>2</sub>O<sub>3</sub> well from standard JCPDS data (39-1346). Characteristic diffraction peaks corresponding to (220), (311), (400), (422), (511), (440), (533) reflections can be found at  $2\theta = 30.241, 35.630, 43.84, 53.733, 57.271, 62.925, 71.820, 74.471$ , respectively. The XPS spectra of  $\alpha$ -Fe<sub>2</sub>O<sub>3</sub>@SiO<sub>2</sub> NPs were also measured as shown in Figure S2 (ESI). It shows that the coating of SiO<sub>2</sub> leads to low Fe<sub>2</sub>O<sub>3</sub> peak intensity.



**Fig. 3** XRD patterns of the  $\alpha$ - $\text{Fe}_2\text{O}_3$ @ $\text{SiO}_2$  and  $\gamma$ - $\text{Fe}_2\text{O}_3$ @ $\text{SiO}_2$  powder with an aspect ratio of 3.

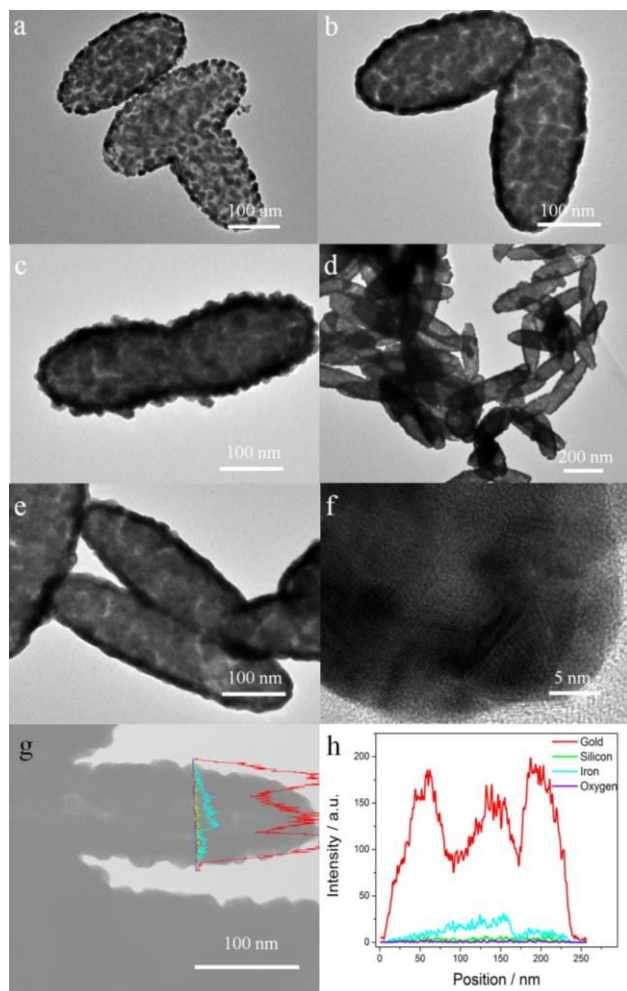
### 3.3 Fabrication of $\gamma$ - $\text{Fe}_2\text{O}_3$ @ $\text{SiO}_2$ @Au NPs

Figure 4 shows TEM images of THPC-Au and  $\gamma$ - $\text{Fe}_2\text{O}_3$ @ $\text{SiO}_2$ @THPC-Au. Figure 4a shows that THPC-Au nanoparticles are rather uniform in size with a mean diameter of  $\sim 3$  nm, which is consistent with the previous report.<sup>31</sup> Figure 4b shows a low magnification TEM image of  $\gamma$ - $\text{Fe}_2\text{O}_3$ @ $\text{SiO}_2$  covered with THPC Au NPs. The SAED pattern of the samples confirms that the spindles are  $\gamma$ - $\text{Fe}_2\text{O}_3$  instead of  $\alpha$ - $\text{Fe}_2\text{O}_3$  as shown in the supporting information (Figure S3, ESI). This is in consistent with the XRD results and the data reported by Guivar *et al.*<sup>37</sup> Figures 4c and d show HRTEM of  $\gamma$ - $\text{Fe}_2\text{O}_3$ @ $\text{SiO}_2$  NPs covered with THPC Au NPs. As can be seen, THPC Au NPs are uniformly distributed on the surface of  $\gamma$ - $\text{Fe}_2\text{O}_3$ @ $\text{SiO}_2$ . This uniform distribution of THPC Au NPs may facilitate the growth of relatively smooth and complete Au shell. The clear crystalline structure with d-spacing of  $\sim 2.36$  Å corresponds to  $\{111\}$  plane of Au (Figure 4d).



**Fig. 4** TEM images of (a) THPC Au; (b)  $\gamma$ - $\text{Fe}_2\text{O}_3$ @ $\text{SiO}_2$  attached with THPC Au; (c) distribution of THPC Au onto  $\gamma$ - $\text{Fe}_2\text{O}_3$ @ $\text{SiO}_2$ ; (d) HRTEM of THPC Au attached onto  $\gamma$ - $\text{Fe}_2\text{O}_3$ @ $\text{SiO}_2$ .

Figure 5 shows the  $\gamma$ - $\text{Fe}_2\text{O}_3$ @ $\text{SiO}_2$ @Au NPs fabricated by the seed growth method. By varying the amount of  $\text{HAuCl}_4$  used in the seed growth process, the shell thickness of Au outer layer can be precisely tuned. The Au shell thickness increases with the amount of Au plating solution (Figures 5a-c). And the shell becomes from incomplete (Figure 5a) to complete (Figure 5b). Figure 5d shows the  $\gamma$ - $\text{Fe}_2\text{O}_3$ @ $\text{SiO}_2$ @Au NPs with an aspect ratio of 6 at low resolution. This indicates the present method is effective since all the NPs were coated with a continuous Au layer. The high-resolution image (Figure 5f) shows that relatively good quality of Au shell can be obtained even with less amount of plating solution. The *energy dispersive* X-ray (EDX) image of the  $\gamma$ - $\text{Fe}_2\text{O}_3$ @ $\text{SiO}_2$ @Au ellipsoids indicate that the Au NPs were grown onto the surface of the  $\gamma$ - $\text{Fe}_2\text{O}_3$ @ $\text{SiO}_2$  (Figures 5g and h). In this study, by changing the amount of Au plating solution, the shell thickness of Au can be tuned from  $\sim 11.5$  nm to  $\sim 15.5$  nm. The adjustable Au thickness can be used to tune the spectra of the resulting core-shell structure. The relatively smooth and complete Au layers can be attributed to many factors, especially the  $\text{SiO}_2$  interlayer. Comparing to the samples fabricated without  $\text{SiO}_2$  layer, the  $\gamma$ - $\text{Fe}_2\text{O}_3$ @ $\text{SiO}_2$ @Au ellipsoids are much smoother (Figure S4, ESI). Figure S3 shows the morphology of  $\text{Fe}_2\text{O}_3$ @Au ellipsoids with different aspect ratios fabricated under the same conditions with that of  $\gamma$ - $\text{Fe}_2\text{O}_3$ @ $\text{SiO}_2$ @Au ellipsoids. The resulting  $\text{Fe}_2\text{O}_3$ @Au ellipsoids have relatively rough sea cucumber-like surface. Therefore, the  $\text{SiO}_2$  layer on the surface of  $\gamma$ - $\text{Fe}_2\text{O}_3$  not only prevents the as-reduced magnetic  $\gamma$ - $\text{Fe}_2\text{O}_3$  from aggregation but also facilitates the surface functionalization of ellipsoids with amino-groups for linking to THPC Au NPs. It also should be pointed out that the current method using CO reduction of Au is advantageous over other methods since the resulting Au shell is relatively complete and smooth.<sup>17, 20, 21, 38, 39</sup>



**Fig. 5** TEM images of  $\gamma\text{-Fe}_2\text{O}_3\text{@SiO}_2\text{@Au}$  NPs (aspect ratio of 3) fabricated with (a) 10  $\mu\text{L}$ , (b) 20  $\mu\text{L}$ , and (c) 30  $\mu\text{L}$  Au plating solution; (d-f)  $\gamma\text{-Fe}_2\text{O}_3\text{@SiO}_2\text{@Au}$  NPs (aspect ratio of 6 fabricated with 20  $\mu\text{L}$  Au plating solution at different magnifications; (g)-(h) EDX of the  $\gamma\text{-Fe}_2\text{O}_3\text{@SiO}_2\text{@Au}$  ellipsoids.

Figure 6 shows the magnetization (M-H) curves of both  $\alpha\text{-Fe}_2\text{O}_3\text{@SiO}_2\text{@Au}$  and  $\gamma\text{-Fe}_2\text{O}_3\text{@SiO}_2\text{@Au}$  ellipsoids measured with SOUID at room temperature. It clearly shows that the  $\gamma\text{-Fe}_2\text{O}_3\text{@SiO}_2\text{@Au}$  ellipsoids have relatively strong ferromagnetic properties while the  $\alpha\text{-Fe}_2\text{O}_3\text{@SiO}_2\text{@Au}$  NPs only have very weak ones, which indicates that the  $\gamma\text{-Fe}_2\text{O}_3\text{@SiO}_2\text{@Au}$  ellipsoids can be actively controlled by the external magnetic field and will be potentially useful for a wide range of applications. The saturation magnetization of  $\gamma\text{-Fe}_2\text{O}_3\text{@SiO}_2\text{@Au}$  NPs was estimated to be 17 emu/g. The photographs of  $\gamma\text{-Fe}_2\text{O}_3\text{@SiO}_2\text{@Au}$  NPs solution before and after adsorption and separation by a magnet were carried out to further confirm the magnetic property of  $\gamma\text{-Fe}_2\text{O}_3\text{@SiO}_2\text{@Au}$  NPs. As shown in Figure S5 (ESI), the clear solution obtained after the separation by a magnet, indicating the magnetic property of  $\gamma\text{-Fe}_2\text{O}_3\text{@SiO}_2\text{@Au}$  NPs.

The  $\gamma\text{-Fe}_2\text{O}_3\text{@SiO}_2\text{@Au}$  ellipsoids prepared in this study is a novel structure with unique magnetoplasmonic property that has never been reported before. Yu and co-authors described the synthesis, characterization and properties of  $\alpha\text{-Fe}_2\text{O}_3\text{@SiO}_2\text{@Au}$

NPs.<sup>18</sup> Peng *et al.* demonstrated the synthesis of spherical  $\gamma\text{-Fe}_2\text{O}_3\text{/SiO}_2\text{/Au}$  magnetic composites with sparse Au nanoparticle on the surface of  $\text{SiO}_2$  layer.<sup>40</sup> Both studies demonstrated the fabrication of spherical structure NPs attached with Au NPs while ours are spindle shape. In addition, there was no continuous Au shell formed in both cases. As mentioned earlier, the spindle structure of our  $\gamma\text{-Fe}_2\text{O}_3\text{@SiO}_2\text{@Au}$  NPs combines the plasmonic properties of both magnetic nanorods and nanoshells in a single structure.<sup>19</sup> This spindle geometry possesses greater structural tunability than either a nanorod or a spherical nanoshell. Therefore, none of the above two studies is identical with the present study. Liz-Marzán *et al.* and Ma *et al.* have reported the fabrication of spindle-like  $\alpha\text{-Fe}_2\text{O}_3\text{@Au}$  NPs, respectively.<sup>20, 21</sup> However, the Au shell is very rough and the optical property is less tunable. In addition, the resulting  $\alpha\text{-Fe}_2\text{O}_3\text{@Au}$  NPs lack the unique magnetoplasmonic property.

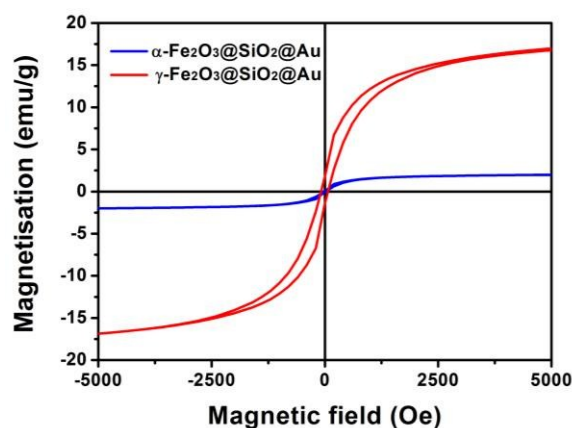


**Fig. 6** Magnetic hysteresis loops of  $\alpha\text{-Fe}_2\text{O}_3\text{@SiO}_2\text{@Au}$  and  $\gamma\text{-Fe}_2\text{O}_3\text{@SiO}_2\text{@Au}$  NPs.

### 3.4 Optical properties of $\gamma\text{-Fe}_2\text{O}_3\text{@SiO}_2\text{@Au}$ NPs

Figure 7 shows the UV-vis-NIR transmission of  $\gamma\text{-Fe}_2\text{O}_3\text{@SiO}_2\text{@Au}$  with different aspect ratios and Au shell thicknesses. The  $\gamma\text{-Fe}_2\text{O}_3\text{@SiO}_2\text{@Au}$  NP with an aspect ratio of 6 shows two peaks. The peaks at longer and shorter wavelengths correspond to the longitudinal and transverse modes of surface plasmons of the  $\gamma\text{-Fe}_2\text{O}_3\text{@SiO}_2\text{@Au}$  ellipsoids, respectively. The peak wavelengths of transverse modes red-shift from 500 to 550 nm when the shell thickness of Au increases for a fixed aspect ratio of 6, while they blue shift for an aspect ratio of 3. This is because the transverse mode also greatly depends on the dielectric properties of the surrounding media and absorption cross section of the NP. From Figure 7, one can observe that for a fixed aspect ratio, the transverse mode of the  $\gamma\text{-Fe}_2\text{O}_3\text{@SiO}_2\text{@Au}$  ellipsoids shows a clear trend, while for different aspect ratios, they may demonstrate either blue shift or red shift. Given that the surrounding media of the Au nanoshell can be considered same for all the NPs, we mainly attribute this difference to the different absorption cross sections of the NPs. The broad longitudinal plasmons remain at the same position when the shell thickness increases from 11.5 nm to 15.5 nm. The strong plasmon

resonance feature observed in the spectra in Figure 7 arises from the longitudinal plasmon of this layered structure and exhibits a highly sensitive structural dependence of its optical resonance, which blue shifts as the metal layer thickness is increased. The  $\gamma$ - $\text{Fe}_2\text{O}_3$ @ $\text{SiO}_2$ @Au NPs possess both magnetic and plasmonic properties, indicating that they could be actively controlled by a magnetic field and hence are important for active plasmonics.<sup>41-43</sup> Figure S6 (ESI) shows the tunable SPR bands under a magnetic field at different angles. The unique magnetoplasmonic properties of such  $\gamma$ - $\text{Fe}_2\text{O}_3$ @ $\text{SiO}_2$ @Au NPs are extremely attractive for SPR sensing as a result of the dipole resonance of the novel nanostructure and recyclable catalysts arising from the outer layer Au shell and magnetic core.<sup>44, 45</sup>

The transmission of  $\gamma$ - $\text{Fe}_2\text{O}_3$ @ $\text{SiO}_2$ @Au NPs is similar with the study conducted by Halas and coworkers except that the broad longitudinal plasmons.<sup>46</sup> It should be pointed out that the samples are measured under different conditions. We measured the transmission spectra of  $\gamma$ - $\text{Fe}_2\text{O}_3$ @ $\text{SiO}_2$ @Au ellipsoids samples that dispersed in  $\text{H}_2\text{O}$  with a UV/Vis/NIR spectrophotometer, whereas in their study, they measured the extinction spectra of monolayers of  $\alpha$ - $\text{Fe}_2\text{O}_3$ @Au isolated nanoshells immobilized on PVP-glass slides with a dark field microscope.

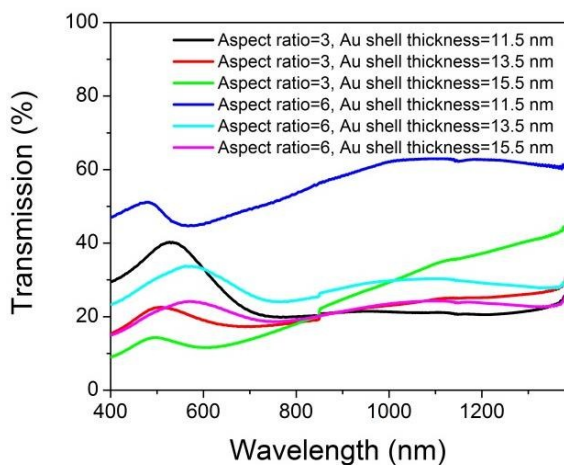


**Fig. 7** Measured transmission spectra of  $\gamma$ - $\text{Fe}_2\text{O}_3$ @ $\text{SiO}_2$ @Au ellipsoids with different aspect ratios and Au shell thicknesses.

We also simulated the optical response of the core-shell structures. A finite difference time domain (FDTD) analysis of the far field scattering spectrum of such a nanostructure reveals that the transverse mode has a much weaker scattering cross section than the longitudinal plasmon mode (Figure 8).<sup>47</sup> In addition, the measured transmission in our experiment could be mainly attributed to the forward scattering of the  $\gamma$ - $\text{Fe}_2\text{O}_3$ @ $\text{SiO}_2$ @Au NPs. From this point of view, the simulated results are in reasonable agreement with the measurements. The difference between the measurement and simulation might be mainly attributed to the shape tolerance and refractive index differences. The refractive index of  $\gamma$ - $\text{Fe}_2\text{O}_3$  was derived by fitting the experimental data in a previous report.<sup>33</sup>

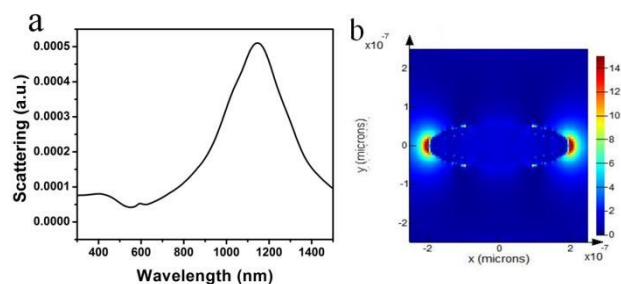


**Fig. 8** (a) Calculated far-field extinction spectrum of the  $\gamma$ - $\text{Fe}_2\text{O}_3$ @ $\text{SiO}_2$ @Au ellipsoids with incident polarization along the longitudinal axis of a nanorice particle using FDTD. The  $\gamma$ - $\text{Fe}_2\text{O}_3$ @ $\text{SiO}_2$ @Au ellipsoids employed for the FDTD simulations is composed of a hematite core with longitudinal diameter of 340 nm and transverse diameter of 54 nm surrounded by a 16-nm-thick Au shell. (b) Near-field profile of the  $\gamma$ - $\text{Fe}_2\text{O}_3$ @ $\text{SiO}_2$ @Au ellipsoids under resonance excitations ( $\lambda_{\text{ex}} = 1148$  nm) with the incident polarization along the longitudinal axis.

## 4. Conclusions

Uniform ellipsoidal  $\alpha$ - $\text{Fe}_2\text{O}_3$ -core@ $\text{SiO}_2$ -interlayer NPs were fabricated by repeating silica coating on the surface of PVP modified hematite spindle cores. By repeating hydrolysis of TEOS, we can obtain ellipsoids with low aspect ratio (<2). Due to the mechanism of hydrolysis of TEOS, polydispersity decreases with increasing the amount of TEOS. These uniform ellipsoids with hematite cores can be transformed into magnetic ones ( $\gamma$ - $\text{Fe}_2\text{O}_3$ @ $\text{SiO}_2$ ) via calcination under  $\text{H}_2$  and then exposure to air.  $\gamma$ - $\text{Fe}_2\text{O}_3$ @ $\text{SiO}_2$ @Au NPs were further fabricated via a seed growth method and characterized using a UV-Vis spectrophotometer. It is found that  $\gamma$ - $\text{Fe}_2\text{O}_3$ @ $\text{SiO}_2$ @Au NPs with large aspect ratios show two peaks. However, for low aspect ratios, there is only one plasmonic resonance peak. In addition, the magnetic  $\gamma$ - $\text{Fe}_2\text{O}_3$ @ $\text{SiO}_2$ @Au NPs could show tailored SPR under a magnetic field, which is useful for fabricating tunable optical nanostructures.<sup>25</sup> The unique magnetoplasmonic properties of this new nanostructure are highly attractive for applications such as SPR sensing because of the dipole resonance of the resultant nanostructure and recyclable catalysts arising from the outer layer Au shell and magnetic core.

## 75 Acknowledgements

The authors thank D. B. Zhou, Z. Q. Li, and Professor. H. T. Dai from Tianjin University to measure the magnetic hysteresis loop of the samples using SQUID. Zhongyu Cai acknowledges a graduate scholarship from the National University of Singapore. We thank the kind help from Professor. Saif Khan and Mr. Prasanna Ganesan K. This work was supported by the joint French-Singaporean MERLION program under Grant No. R-279-000-334-133 and Agency for Science, Technology and Research (A\*STAR) under Grant No. 0921540099 and 0921540098.

## Notes and references

- <sup>a</sup> Department of Chemical and Biomolecular Engineering, National University of Singapore, 4 Engineering Drive 4, Singapore 117585  
Fax: +65-6779-1936; Tel: +65-6516-1071; E-mail: [chelxm@nus.edu.sg](mailto:chelxm@nus.edu.sg)
- <sup>b</sup> Department of Chemistry, University of Pittsburgh, Pittsburgh, Pennsylvania, 15260, United States Tel: +1-412-624-6313; E-mail: [chemczy@gmail.com](mailto:chemczy@gmail.com)
- <sup>c</sup> Institute of Materials Research and Engineering, Agency for Science, Technology and Research (A\*STAR), 3 Research Link, Singapore 117602  
Fax: +65-6872-0785; Tel: +65-6874-8137; E-mail: [jh-teng@imre.a-star.edu.sg](mailto:jh-teng@imre.a-star.edu.sg); Tel: +65-6513-1358; Email: [liuy@imre.a-star.edu.sg](mailto:liuy@imre.a-star.edu.sg)
- <sup>d</sup> CNRS, Univ. Bordeaux, CRPP, UPR 8641, F-33600 Pessac, France.
- † Electronic Supplementary Information (ESI) available: SEM images of  $\alpha$ -Fe<sub>2</sub>O<sub>3</sub> NPs, summary of the average size and size distribution of  $\alpha$ -Fe<sub>2</sub>O<sub>3</sub> NPs, XPS spectra of  $\alpha$ -Fe<sub>2</sub>O<sub>3</sub> NPs, TEM images of  $\alpha$ -Fe<sub>2</sub>O<sub>3</sub>@Au NPs, SAED patterns of  $\gamma$ -Fe<sub>2</sub>O<sub>3</sub>@SiO<sub>2</sub>, photographs of  $\gamma$ -Fe<sub>2</sub>O<sub>3</sub>@SiO<sub>2</sub>@Au NPs solution before and after adsorption and separation by a magnet and transmission spectra of  $\gamma$ -Fe<sub>2</sub>O<sub>3</sub>@SiO<sub>2</sub>@Au ellipsoids in a magnetic field with different angles along their longitudinal direction. See DOI: 10.1039/b000000x/
- ## References
- A. O. Govorov and H. H. Richardson, *Nano Today*, 2007, **2**, 30-38.
  - N. J. Halas, S. Lal, W.-S. Chang, S. Link and P. Nordlander, *Chem. Rev.*, 2011, **111**, 3913-3961.
  - V. Giannini, A. I. Fernández-Domínguez, S. C. Heck and S. A. Maier, *Chem. Rev.*, 2011, **111**, 3888-3912.
  - M. B. Cortie and A. M. McDonagh, *Chem. Rev.*, 2011, **111**, 3713-3735.
  - S. Lal, N. K. Grady, J. Kundu, C. S. Levin, J. B. Lassiter and N. J. Halas, *Chem. Soc. Rev.*, 2008, **37**, 898-911.
  - R. Bardhan, S. Lal, A. Joshi and N. J. Halas, *Acc. Chem. Res.*, 2011, **44**, 936-946.
  - H. Wang, L. Chen, Y. Feng and H. Chen, *Acc. Chem. Res.*, 2013, **46**, 1636-1646.
  - P. K. Jain, I. H. El-Sayed and M. A. El-Sayed, *Nano Today*, 2007, **2**, 18-29.
  - Y. B. Zheng, B. Kiraly, P. S. Weiss and T. J. Huang, *Nanomedicine*, 2012, **7**, 751-770.
  - J. S. Chen, C. M. Li, W. W. Zhou, Q. Y. Yan, L. A. Archer and X. W. Lou, *Nanoscale*, 2009, **1**, 280-285.
  - Z. Wang, D. Luan, S. Madhavi, Y. Hu and X. W. Lou, *Energy Environ. Sci.*, 2012, **5**, 5252-5256.
  - Z. Cai, Z. Xiong, X. Lu and J. Teng, *J. Mater. Chem. A*, 2014, **2**, 545-553.
  - R. Ghosh Chaudhuri and S. Paria, *Chem. Rev.*, 2011, **112**, 2373-2433.
  - S. J. Oldenburg, R. D. Averitt, S. L. Westcott and N. J. Halas, *Chem. Phys. Lett.*, 1998, **288**, 243-247.
  - H. Wang, D. W. Brandl, F. Le, P. Nordlander and N. J. Halas, *Nano Lett.*, 2006, **6**, 827-832.
  - B. Sepúlveda, P. C. Angelomé, L. M. Lechuga and L. M. Liz-Marzán, *Nano Today*, 2009, **4**, 244-251.
  - B. E. Brinson, J. B. Lassiter, C. S. Levin, R. Bardhan, N. Mirin and N. J. Halas, *Langmuir*, 2008, **24**, 14166-14171.
  - F. Chun-Liu, Q. Kun, Z. Jianhua, W. Shangbin, L. Xiaoxuan and Y. Shu-Hong, *Nanotechnology*, 2008, **19**, 125601.
  - Z. Li, M. Peng, Y. Jin, X. Wang, Y. Cui and C. Chen, *Chin. Sci. Bull.*, 2011, **56**, 2911-2915.
  - M. Spuch-Calvar, J. Pérez-Juste and L. M. Liz-Marzán, *J. Colloid Interface Sci.*, 2007, **310**, 297-301.
  - Z. Ma, H. Han, S. Tu and J. Xue, *Colloids Surf., A*, 2009, **334**, 142-146.
  - N. Phonthammachai, J. C. Y. Kah, G. Jun, C. J. R. Sheppard, M. C. Olivo, S. G. Mhaisalkar and T. J. White, *Langmuir*, 2008, **24**, 5109-5112.
  - R. Bardhan, O. Neumann, N. Mirin, H. Wang and N. J. Halas, *ACS Nano*, 2009, **3**, 266-272.
  - Z. Cai, Y. J. Liu, X. Lu and J. Teng, *J. Phys. Chem. C*, 2013, **117**, 9440-9445.
  - M. Wang, C. Gao, L. He, Q. Lu, J. Zhang, C. Tang, S. Zorba and Y. Yin, *J. Am. Chem. Soc.*, 2013, **135**, 15302-15305.
  - H. Giesche, *J. Eur. Ceram. Soc.*, 1994, **14**, 205-214.
  - Z. Cai, J. Teng, D. Xia and X. S. Zhao, *J. Phys. Chem. C*, 2011, **115**, 9970-9976.
  - Z. Y. Cai, Y. J. Liu, X. M. Lu and J. H. Teng, *ACS Appl. Mater. Interfaces*, 2014, **6**, 10265-10273.
  - M. Ocaña, M. P. Morales and C. J. Serna, *J. Colloid Interface Sci.*, 1999, **212**, 317-323.
  - T. Ding, K. Song, K. Clays and C.-H. Tung, *Adv. Mater.*, 2009, **21**, 1936-1940.
  - D. G. Duff, A. Baiker and P. P. Edwards, *Langmuir*, 1993, **9**, 2301-2309.
  - S. L. Westcott, S. J. Oldenburg, T. R. Lee and N. J. Halas, *Langmuir*, 1998, **14**, 5396-5401.
  - M. Gartner, M. Crisan, A. Jitianu, R. Scurtu, R. Gavrilă, I. Oprea and M. Zaharescu, *J. Sol-Gel Sci. Technol.*, 2003, **26**, 745-748.
  - C. Graf, D. L. J. Vossen, A. Imhof and A. van Blaaderen, *Langmuir*, 2003, **19**, 6693-6700.
  - Z. Cai, J. Teng, Q. Yan and X. S. Zhao, *Colloids Surf., A*, 2012, **402**, 37-44.
  - Z. Cai, Y. J. Liu, E. S. P. Leong, J. Teng and X. Lu, *J. Mater. Chem.*, 2012, **22**, 24668-24675.
  - J. Guivar, Martínez, A., Anaya, A., Valladares, L., Félix, L., Domínguez, A., *Adv. Nanopart.*, 2014, **3**, 114-121.
  - N. Phonthammachai, J. C. Y. Kah, G. Jun, C. J. R. Sheppard, M. C. Olivo, S. G. Mhaisalkar and T. J. White, *Langmuir*, 2008, **24**, 5109-5112.
  - X. Xu and M. B. Cortie, *J. Phys. Chem. C*, 2007, **111**, 18135-18142.
  - Z. X. Li, M. L. Peng, Y. Y. Jin, X. F. Wang, Y. L. Cui and C. Chen, *Chin. Sci. Bull.*, 2011, **56**, 2911-2915.
  - V. K. S. Hsiao, Y. B. Zheng, B. K. Juluri and T. J. Huang, *Adv. Mater.*, 2008, **20**, 3528-3532.
  - G. Armelles, A. Cebollada, A. García-Martín and M. U. González, *Adv. Opt. Mater.*, 2013, **1**, 10-35.
  - G. Y. Si, Y. H. Zhao, E. S. P. Leong and Y. J. Liu, *Materials*, 2014, **7**, 1296-1317.
  - J. Homola, *Chem. Rev.*, 2008, **108**, 462-493.
  - Z. Xuming, C. Yu Lim, L. Ru-Shi and T. Din Ping, *Rep. Prog. Phys.*, 2013, **76**, 046401.
  - H. Wang, D. W. Brandl, F. Le, P. Nordlander and N. J. Halas, *Nano Lett.*, 2006, **6**, 827-832.
  - C. Oubre and P. Nordlander, *J. Phys. Chem. B*, 2004, **108**, 17740-17747.

Cite this: DOI: 10.1039/c0xx00000x

www.rsc.org/xxxxxx

ARTICLE TYPE

## Sandwich-structured $\text{Fe}_2\text{O}_3@\text{SiO}_2@\text{Au}$ nanoparticles with magnetoplasmonic responses

Zhongyu Cai,<sup>a,b\*</sup> Eunice S. P. Leong,<sup>c</sup> Zhigang Wang,<sup>a</sup> Wenxin Niu,<sup>a</sup> Weiqing Zhang,<sup>a</sup> Serge Ravaine,<sup>d</sup> Nikolai L. Yakovlev,<sup>c</sup> Yan Jun Liu,<sup>c\*</sup> Jinghua Teng,<sup>c\*</sup> Xianmao Lu<sup>a\*</sup>

<sup>5</sup> Received (in XXX, XXX) Xth XXXXXXXXX 20XX, Accepted Xth XXXXXXXXX 20XX

DOI: 10.1039/b000000x

### Graphic abstract

We fabricated highly uniform sandwich-structured  $\gamma\text{-Fe}_2\text{O}_3@\text{SiO}_2@\text{Au}$  spindle nanoparticles with novel structural and magnetic tunable surface plasmon resonance.

10

